5-1-2022

Characterizing Sensitive Cardiac Substructure Excursion Due to Respiration

Claudia R. Miller

Eric D. Morris

Ahmed I. Ghanem

Milan V. Pantelic

Eleanor M. Walker

See next page for additional authors

Authors

Claudia R. Miller, Eric D. Morris, Ahmed I. Ghanem, Milan V. Pantelic, Eleanor M. Walker, and Carri K. Glide-Hurst

Scientific Article

Characterizing Sensitive Cardiac Substructure Excursion Due to Respiration

Claudia R. Miller, BSE,[a] Eric D. Morris, PhD,[a] Ahmed I. Ghanem, MD, PhD,[b,c]
Milan V. Pantelic, MD,[d] Eleanor M. Walker, MD,[c] and
Carri K. Glide-Hurst, PhD[e,*]

[a]Department of Radiation Oncology, University of California—Los Angeles, Los Angeles, California; [b]Alexandria Clinical Oncology Department, Alexandria University, Alexandria, Egypt; [c]Department of Radiation Oncology, Henry Ford Cancer Institute, Detroit, Michigan; [d]Department of Radiology, Henry Ford Health System, Detroit, Michigan; [e]Department of Human Oncology, School of Medicine and Public Heath, University of Wisconsin—Madison, Madison, Wisconsin

Abstract

Purpose: Whole-heart dose metrics are not as strongly linked to late cardiac morbidities as radiation doses to individual cardiac substructures. Our aim was to characterize the excursion and dosimetric variation throughout respiration of sensitive cardiac substructures for future robust safety margin design.

Methods and Materials: Eleven patients with cancer treatments in the thorax underwent 4-phase noncontrast 4-dimensional computed tomography (4DCT) with T2-weighted magnetic resonance imaging in end-exhale. The end-exhale phase of the 4DCT was rigidly registered with the magnetic resonance imaging and refined with an assisted alignment surrounding the heart from which 13 substructures (chambers, great vessels, coronary arteries, etc) were contoured by a radiation oncologist on the 4DCT. Contours were deformed to the other respiratory phases via an intensity-based deformable registration for radiation oncologist verification. Measurements of centroid and volume were evaluated between phases. Mean and maximum dose to substructures were evaluated across respiratory phases for the breast (n = 8) and thoracic cancer (n = 3) cohorts.

Results: Paired *t* tests revealed reasonable maintenance of geometric and anatomic properties (*P* < .05 for 4/39 volume comparisons). Maximum displacements >5 mm were found for 24.8%, 8.5%, and 64.5% of the cases in the left-right, anterior-posterior, and superior-inferior axes, respectively. Vector displacements were largest for the inferior vena cava and the right coronary artery, with displacements up to 17.9 mm. In breast, the left anterior descending artery D_{mean} varied 3.03 ± 1.75 Gy (range, 0.53-5.18 Gy) throughout respiration whereas lung showed patient-specific results. Across all patients, whole heart metrics were insensitive to breathing phase (mean and maximum dose variations <0.5 Gy).

Conclusions: This study characterized the intrafraction displacement of the cardiac substructures through the respiratory cycle and highlighted their increased dosimetric sensitivity to local dose changes not captured by whole heart metrics. Results suggest value of cardiac substructure margin generation to enable more robust cardiac sparing and to reduce the effect of respiration on overall treatment plan quality.

Introduction

Radiation dose to the heart from thoracic cancer radiation therapy (RT) may increase risks of ischemic heart disease, cardiomyopathy, and artery atherosclerosis.[1,2] Currently, only whole heart dose/volume estimates are considered for RT planning in clinical practice.[3] Recent studies have shown that dose to individual substructures may be better indicators of future cardiac events than whole heart dose metrics.[4] A present challenge of improving cardiac substructure sparing during the treatment planning process is that they are difficult to discern on standard computed tomography (CT) simulation scans. High resolution CT coronary angiography drastically improves the visualization of the coronary arteries,[5] although CT coronary angiography is most commonly used to evaluate vascular disease[6] and also requires the use of contrast. Magnetic resonance imaging (MRI) provides soft tissue discrimination and allows for substructure visualization. However, cardiac MRIs and MRIs acquired of the thoracic region are not standard of care for radiation treatment planning due to high costs, accessibility limitations, and technical challenges introduced by susceptibility artifacts caused by air-tissue interfaces.[7]

Aside from localizing cardiac substructures for initial treatment planning, assessing dose and developing cardiac spared plans may be further complicated by substructure intrafraction motion. Guzhva et al[8] evaluated 10-phase 4-dimensional (4D) CTs to analyze the combined intrafractional cardiac and respiratory motion of 12 cardiac substructures for 20 patients undergoing RT for thoracic cancers. Substructure segmentations were completed on the 50% phase (end-exhalation [EE]) and then deformably propagated to the remaining phases.[8] They found that the largest centroid displacements from intrafractional motion were in the superior-inferior (S-I) axis and that the cardiac chambers yielded the smallest displacements overall (largest displacements in the coronary vessels).[8]

Several studies have reported on the dosimetric effect of intrafractional motion on the heart during thoracic cancer RT. A study by George et al[9] studied the effects of intrafraction motion for breast cancer treatments using intensity modulated radiation therapy under shallow, normal, and deep breathing conditions and found that heart dose/volumetric endpoints increased with increased respiratory excursion. Similarly, Yue et al[10] evaluated the effect of intrafraction motion arising from respiration on dose-volume histogram metrics for left breast cancer treatments using 10-phase 4DCT, revealing that maximum heart doses varied up to 6 Gy under normal respiratory conditions. El-Sherif et al[11] evaluated 10-phase 4DCTs for intrafraction motion evaluation of left-sided breast cancer treatments and included the whole heart, left ventricle (LV), and left anterior descending artery (LADA). This work revealed that although the 95% confidence interval of the 4D dose was ±0.5 Gy for the whole heart, it varied ±8.7 Gy for the LADA, thus underscoring the importance of evaluating dose to individual cardiac substructures and the potential sensitivity to the effects of respiration.

This work sought to (1) quantify the excursion of 13 cardiac substructures during respiration by applying segmentation pipelines to 4DCT data coupled with deformable image registration (DIR) and (2) examine areas of potential dosimetric effect. Our study builds upon the current literature by providing population results and including additional substructures, such as the left main coronary artery (LMCA) and the great vessels (ie, superior vena cava [SVC], ascending aorta [AA], and pulmonary artery [PA]). Additionally, the current study provides volume and dose statistics across respiratory phases. When combined with interfraction uncertainties and cardiac motion assessments, a robust safety margin for cardiac substructures can be defined to ensure adequate cardiac sparing.

Methods and Materials

Patient cohort and imaging

Eleven patients with cancer were retrospectively reviewed in an institutional review board approved study conducted at the Henry Ford Cancer Institute. Detailed demographic and treatment-related information for each patient included in our study is outlined in Table 1. These patients either underwent 4-phase (n = 8, patients with breast cancer) or 10-phase (n = 3, patients with lesions in the thoracic region) noncontrast 4DCTs. All initial dose calculations and treatment planning were conducted on the average CT per our standard clinical workflow. All patients were imaged with a respiratory correlated 4DCT and cardiac gated T2-weighted MR in EE. Reconstructed data were exported from the clinical scanners and deidentified for analysis. The EE phase of the 4DCT was rigidly registered with the EE MRI and the registration was refined with an assisted alignment surrounding the heart using MIM (version 6.9.1; MIM Software Inc, Cleveland, OH).

Autosegmentation

Thirteen cardiac substructures including the heart, LV/right ventricle, left atrium/right atrium (RA), pulmonary vein, PA, AA, SVC/inferior vena cava (IVC), LADA, LMCA, and right coronary artery (RCA) were automatically segmented using multiatlas[12] (n = 8) and deep learning techniques[13] (n = 3) that used hybrid MRI/CT information on the EE phase of the 4DCTs. These EE delineations were verified and, if needed, corrected by a

Table 1   Description of each patient case outlining gender, age, tumor histology, staging, tumor location, dose in Gy per fx, and treatment technique

Patient	Sex	Age	Histology	Stage	Location	Dose (Gy/fx)	Technique
1	F	46	Invasive ductal carcinoma	IIIA	Breast	61.2/34	3D
2	F	64	Invasive ductal carcinoma	IA	Breast	52.72/21	3D
3	F	68	Invasive ductal carcinoma	IA	Breast	50.72/21	3D
4	F	59	Invasive lobular carcinoma	IIIC	Breast	50/25	3D
5	F	67	Invasive ductal carcinoma	IIA	Breast	61.2/34	3D
6	F	70	Invasive ductal carcinoma	IA	Breast	52.72/21	3D
7	F	48	Invasive ductal carcinoma	II	Breast	61.2/34	3D
8	F	61	Intraductal carcinoma in situ	0	Breast	52.72/21	3D
9	M	89	Small cell lung cancer	IIIA	Thorax	60/20	IMRT
10	M	73	High-grade pleomorphic sarcoma	IIA	Thorax	50/5	SBRT
11	M	69	Adenocarcinoma	IA	Thorax	48/4	SBRT

Abbreviations: 3D = 3-dimensional conformal; F = female; fx = fraction; IMRT = intensity modulated radiation therapy; M = male; SBRT = stereotactic body radiation therapy.

physician before propagating contours to the other phases. All initial physician delineations and subsequent corrections followed a consensus contouring guideline for cardiac segmentation.[14]

Figure 1 best summarizes the methods used for characterization of cardiac substructure excursion due to respiration. Physician-verified contours on the EE of the 4DCT were deformed to the other phases using a constrained, intensity-based, free-form DIR based on Demons, which minimizes the intensity differences between 2 single modality data sets.[15] Demons algorithms are widely used for their accuracy and computational efficiency.[16,17] This same DIR algorithm from MIM software has been implemented in several other CT to CT DIR studies[18-20] and has been reported to have a ∼1-mm error from gold standard deformations.[21] To conduct the DIR, a box-based assisted alignment around the heart was first completed. The DIR workflow creates a set of grid control points using a coarse-to-fine, multiresolution approach that has been shown to allow for anatomic alignment even when large differences are present due to respiration.[18] Regularization was also implemented to minimize folds and tears in the deformation field.[18] Once the DIR was used to propagate segmentations to each phase of the 4DCT, final contour verification was conducted by a radiation oncologist. Final analysis was conducted to define the location of each cardiac substructure at end-inhalation (0%), EE (50%), and 2 intermediate breathing phases (25%-30%, 70%-75%).

Analysis for statistical and quantitative comparisons

Measurements of centroid and volume at each respiratory phase were exported from MIM for subsequent analysis. Maximum excursions in each direction were calculated and reported as mean ± standard deviation. Displacements >5 mm for each of the 3 cardinal axes were evaluated based on guidance provided by the respiratory motion management report produced by the American Association of Physicist in Medicine Task Group report 76.[22] Paired t tests were employed for statistical analysis of each substructure to compare contour volumes across phases. Any P value < 0.05 was considered a statistically significant difference. All statistical analysis was performed using SPSS version 25.0 (SPSS, Chicago, IL).

Dosimetric analysis

To quantify differences in dosimetric endpoints, clinically approved treatment plans were transferred to the evaluated phases of the 4DCTs (ie, 0%, 25%-30%, 50%, and 70%-75%). The mean (D_{mean}) and maximum doses (D_{max}) were tabulated for each substructure and the largest dosimetric changes over the respiratory phases were quantified. As the patient cohort consisted of breast and thoracic cancer cohorts, percent dose variation over the respiratory cycle was quantified.

Results

Cardiac substructure displacement

Centroid displacements for the left-right (L-R), anterior-posterior (A-P), S-I, and vector shifts for the patient population are shown in Figure 2. The location of each cardiac substructure at end-inhalation (0%), EE (50%), and 2 intermediate phases (25%-30%, 70%-75%) were
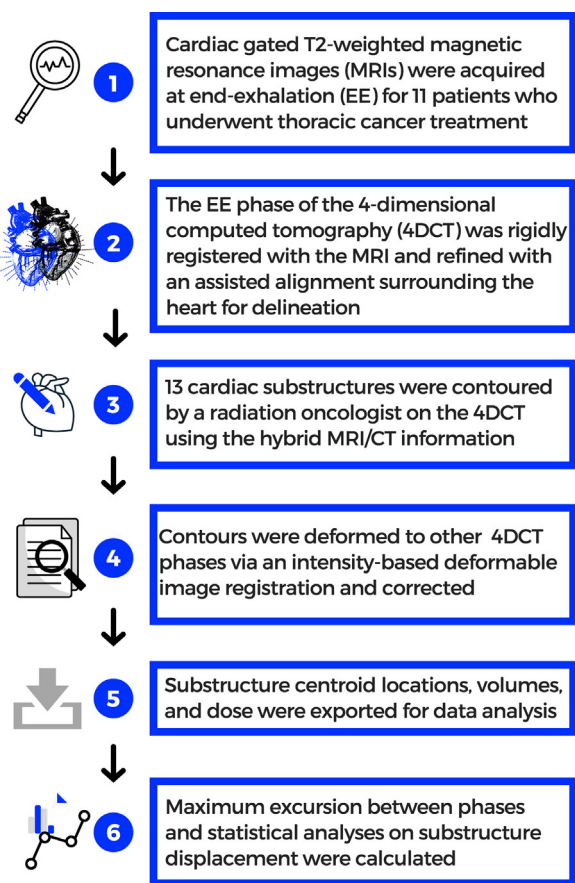
Figure 1 Methods for characterization of cardiac substructure excursion due to respiration.

evaluated in this study. The maximum vector displacements ranged from 5 to 10 mm across most substructures, with the largest displacements occurring for the IVC and the RCA with displacements up to 17.9 mm. Of the 3 cardinal axes, intrafraction centroid displacements were the largest in the S-I axis. Maximum displacements of >5 mm were found for 24.8%, 8.5%, and 64.5% of the cases in the L-R, A-P, and S-I axes, respectively. As shown by the boxplots in Figure 2, 10/13 substructures had median intrafraction S-I centroid displacements ≥5 mm. Further, only the S-I axis had a 95th data percentile that extended past 15 mm (ie, IVC). For 10/13 studied cardiac structures, data for the first 3 quartiles were <5 mm in the L-R axis. With regard to outliers, 8/9 outliers in the L-R axis can be attributed to a single patient. Over all substructures, the A-P axis exhibited the least excursion. As shown in Figure 2, median excursions for 11/13 structures were smallest in the A-P axis. Table 2 also summarizes the L-R, A-P, and S-I maximal displacements for each cardiac substructure over the patient population.

When considering regional location of particular substructures, Table 2 reveals that the great vessels (ie, the AA, SVC, and PA) exhibited the least amount of excursion along each axis, which was also confirmed by Figure 2. Both the IVC and the RCA, which are located at the inferior aspect of the heart, had maximal centroid displacements that were >15 mm. Data presented in Figure 2 and Table 2 also reveal that the IVC was the substructure with the largest displacements in the S-I axis. For the RCA, 9/11 patients had S-I displacements >5 mm whereas the IVC had 8 patients exceed this threshold. The

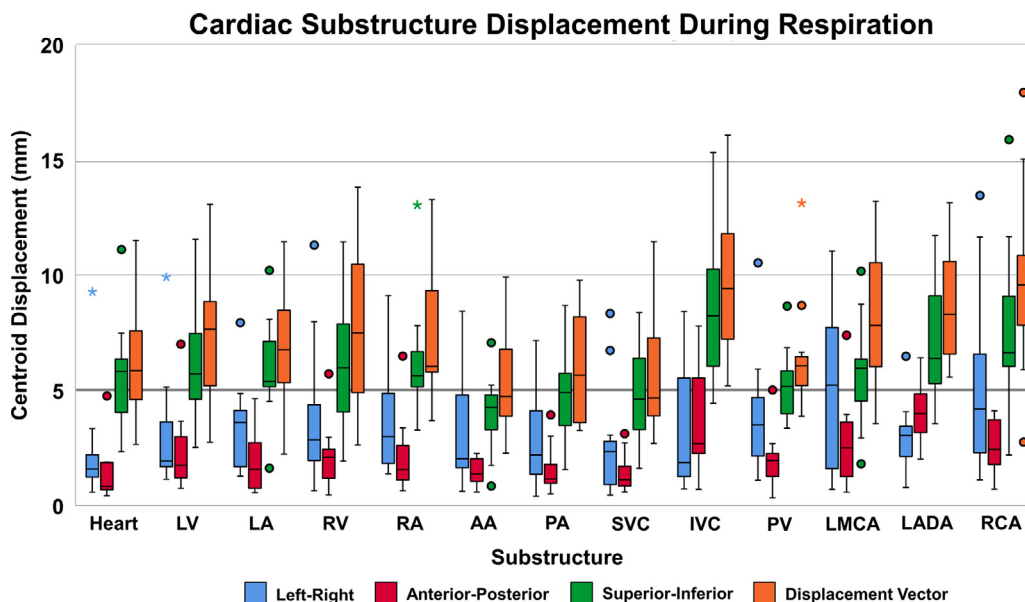**Figure 2** Intrafraction centroid displacement comparison between all 13 structures for each direction: left-right, anterior-posterior, superior-inferior, and vector. Boxplots, thick line, and whiskers represent the interquartile range (IQR), median, and 5th and 95th percentiles, respectively. Data points displayed as a small circle represent a value >1.5 times the IQR and the star represents a value >3 times the IQR.

Table 2 Maximum displacement of individual cardiac substructures over 11 patients throughout the respiratory cycle in each cardinal axis (left-right (L-R), anterior-posterior (A-P), and superior-inferior (S-I)) and vector displacements. Substructure abbreviations defined in the text.

Substructure	L-R (mm)	A-P (mm)	S-I (mm)	Vector (mm)
Heart (n=9)	2.5 ± 2.7	1.5 ± 1.4	5.9 ± 2.5	6.6 ± 3.1
LV	3.1 ± 2.6	2.4 ± 1.8	6.3 ± 2.8	7.6 ± 3.4
LA	3.4 ± 2.0	1.9 ± 1.3	6.0 ± 2.2	7.0 ± 2.7
RV	3.9 ± 3.1	2.1 ± 1.4	6.1 ± 3.0	7.7 ± 3.6
RA	3.7 ± 2.5	2.1 ± 1.7	6.2 ± 2.6	7.5 ± 3.1
PA	2.9 ± 2.2	1.6 ± 1.1	4.9 ± 2.0	6.0 ± 2.5
AA	3.1 ± 2.5	1.4 ± 0.6	4.0 ± 1.7	5.4 ± 2.4
SVC	2.8 ± 2.6	1.4 ± 0.9	5.0 ± 2.3	5.7 ± 2.8
PV	3.9 ± 2.6	2.0 ± 1.2	5.2 ± 1.6	6.5 ± 2.5
IVC	3.2 ± 2.7	3.8 ± 2.5	8.5 ± 3.3	9.8 ± 3.4
RCA	5.3 ± 4.1	2.6 ± 1.2	7.8 ± 3.7	9.8 ± 4.1
LADA	3.0 ± 1.5	4.1 ± 1.3	7.1 ± 2.6	8.7 ± 2.5
LMCA	5.0 ± 3.5	2.7 ± 2.0	5.8 ± 2.4	8.2 ± 3.1
Individual Cardiac Substructure Excursion in Respiration				

RCA and IVC each had the largest maximum vector displacements of >9 mm, as summarized in Table 2.

4DCT excursion analysis revealed that 52.5% and 31.9% of the maximum excursions over the respiratory cycle occurred between the 0 and 50% and the 0 and 70% (or 75%) trajectories, respectively. Maximum excursions only occurred between the 0 and 30% (or 25%) phases 6.4% (9/141 instances) of the time.

Figure 3 shows substructure excursion between the 0% (bottom row) and the 50% phase (top row) for 2 representative patients in both the axial and sagittal axes. Patient 1 (Fig 3, left) exhibited minimal substructure centroid displacement over the respiratory cycle. Patient 1 had smaller than average vector displacements for 11/13 cardiac structures (LMCA had the largest vector excursion for this patient of 11.8 mm). Even though the largest displacements were observed in the S-I axis across the population, patient 9 presented as an outlier that underwent the largest L-R displacement across the cohort, with L-R intrafraction displacements for 12/13 substructures exceeding the Task Group (TG)-76 motion management recommendation of 5 mm and an LADA displacement of up to 13.5 mm and in the S-I axis centroid displacements for all substructures >5.0 mm and up to 8.7 mm.

Volume and statistical analysis

The paired t tests revealed that out of 39 volume comparisons per patient (13 substructures, 4 phases), there were only 4 instances with statistically significant differences ($P < .05$) for the volume comparisons, suggesting

reasonable maintenance of geometric and anatomic properties. The average volume of the whole heart across all patients at the 50% phase was 718.6 ± 133.4 cc. On average, the percent difference in volume for the whole heart between the 0% and 50% phases was 1.2 ± 0.5%. The cardiac substructures with the largest variabilities in volume between EE and end-inhale (EI) had average volumes >70 cc (PA and chambers), as shown in Appendix E1. The RA had the largest volume differences between EE and EI of 7.8 ± 6.5% (range, 0.9%-20.2%).

Dosimetric analysis

Over the 8 studied patients with breast cancer, the LADA D_{mean} varied 3.03 ± 1.75 Gy (range, 0.53-5.18 Gy) whereas the whole heart D_{mean} changed 0.18 ± 0.09 Gy (range, 0.06-0.37 Gy) during respiration. Boxplots shown in Figure 4 best summarize the mean doses to each individual substructure between end-inhalation (0% 4DCT phase) and EE (50% 4DCT phase) for the left breast cancer cohort, highlighting that the most dominant differences were observed for the LADA.

The dose-volume histograms shown in Figure 5 across the 3 patients with lung cancer highlight patient-specific results. Of the 3 patients with thoracic cancer studied, patient 9 experienced the largest changes in dose across respiratory phases (average change in D_{max} of 3.2 ± 2.9 Gy [range, 0.46 PA-9.05 Gy RA] and D_{mean} was 2.2 ± 1.8 Gy across cardiac substructures). For the other 2 patients with thoracic cancer treated with stereotactic body radiation therapy,
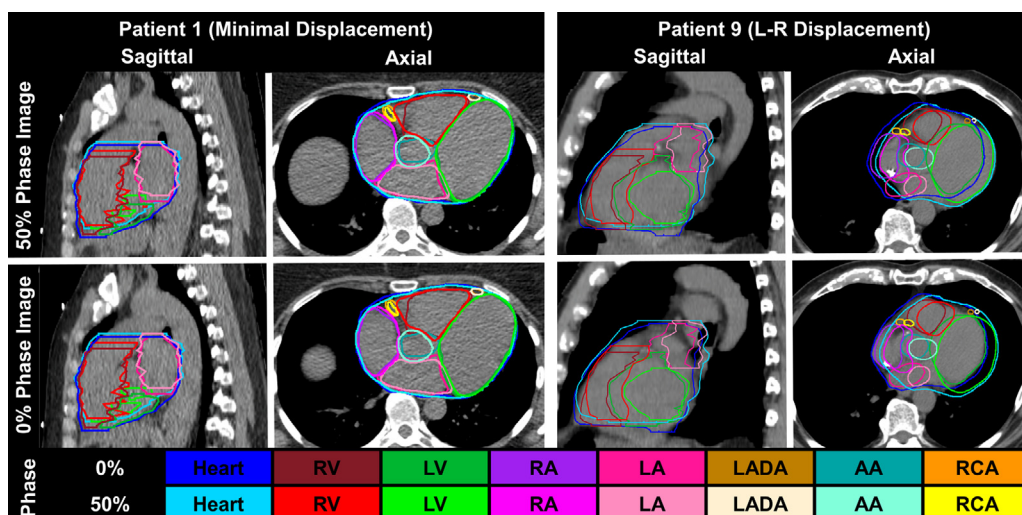
Figure 3   Two representative patients showing substructure excursion between 0% (bottom row) and 50% phase (top row) images with the contours from each phase shown on both image sets for the axial and the sagittal axes. Left: patient 1 selected for minimal displacement over respiration. Right: patient 9 chosen for largest left-right (L-R) displacement across patients. Cardiac substructure abbreviations are defined in the text.

no cardiac substructure had D_{mean} differences >1.4 Gy (D_{max} differences up to 5.6 Gy).

To show this in additional detail, Appendix E1 shows 2 representative patients with breast cancer with the heart, ventricles, and LADA displayed over respiratory phases. Both patient 2 and patient 6 were treated to 42.72 Gy in 16 fractions for a stage 1A malignant neoplasm of the left breast. For these patients, the LADA (Appendix E1, green) had a D_{mean} that varied >3.5 Gy over the respiratory cycle.

Discussion

By leveraging multiphase 4DCT data, this work sought to quantify the intrafractional displacements of sensitive cardiac substructures and summarize the dosimetric effect throughout the respiratory cycle. Although other studies have focused on intrafraction displacement of the whole heart, our work further quantified displacement for additional cardiac substructures. Our methodology of using 4DCT and DIR was similar to a study by Guzhva et al,[8] where contours were propagated from the 50% phase to the other phases and then manually revised. They found that vector intrafractional displacement of the cardiac substructures ranged from 7 to 15 mm and was dominant in the S-I axis.[8] Our work agrees with these findings in that substructure excursion from respiration was predominant in the S-I axis, and maximal vector displacements ranged from 5 to 10 mm. Our study built on the work conducted by Guzhva et al[8] by considering the LMCA and the LADA as separate cardiac substructures and through the consideration of the great vessels (ie, SVC, PA, and AA). This work also characterizes the dosimetric

effect at different phases in respiration for both breast and thoracic cancer cases. However, both studies were limited, as neither accounted for interobserver contouring variability and interfraction uncertainties.

This work found that substructures toward the superior extent of the heart, the great vessels (ie, AA, SVC, and PA), had the smallest displacements in each axis, whereas substructures at the inferior extent of the heart, the RCA and the IVC, had the largest displacements. Limited cardiac substructure excursion data are available for direct comparison; however, it has been reported that tumor excursion in inferior lung lobes displaces the most over the respiratory cycle.[23,24] In the present study, the largest substructure centroid displacements occurred for the IVC, which is located at the inferior aspect of the heart and passes through the diaphragm at the vena caval foramen.[25]

Moreover, the dosimetric analysis conducted to evaluate the effect of breathing phase on substructure dose revealed that although changes in D_{mean} and D_{max} for the heart were less sensitive to respiration (<0.5 Gy), large dose differences for individual substructures were observed. Figure 4 highlights the varied sensitivity of the mean cardiac substructure doses with respiration for the breast cancer cohort with the LADA D_{mean} varying ∼3 Gy during respiration across the population. Figure 5 demonstrates the effect of breathing phase on substructure dose for 3 patients with lung cancer. Patient 9 shows mean dose differences of >3 Gy with respiration for the AA, LMCA, pulmonary vein, and SVC with effect of respiration >8 Gy for the maximum doses to the AA and RA. In a recent retrospective analysis of >700 patients with locally advanced non-small lung cancer, after controlling for baseline risk factors, radiation dose to several cardiac substructures,
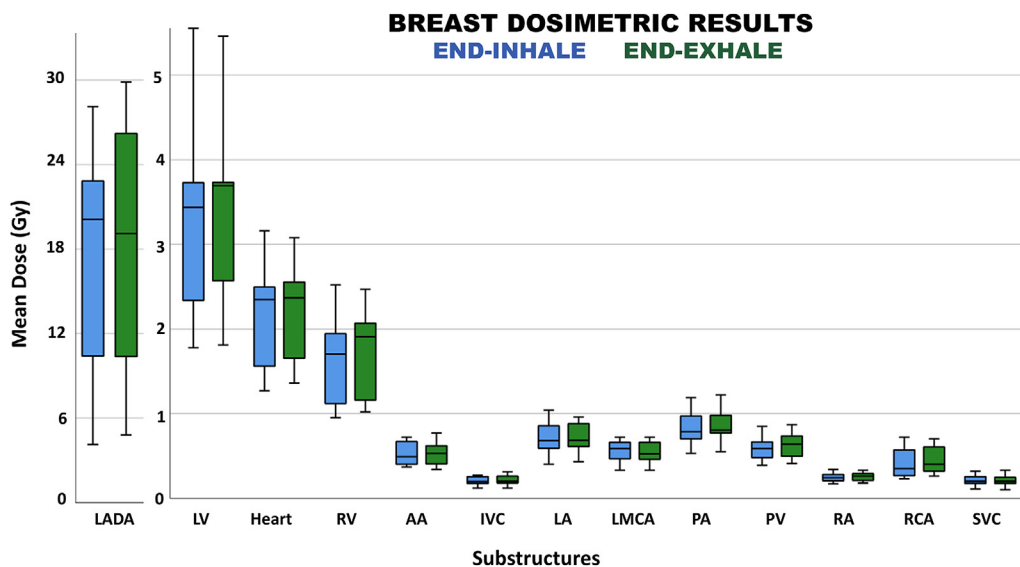
Figure 4 Mean doses to individual substructures (abbreviations defined in the text) for the patient with breast cancer cohort highlighting the dosimetric variation observed between end-inhalation (0% 4-dimensional computed tomography [4DCT] phase) and end-exhalation (50% 4DCT phase).

including mean total coronary dose ≥7 Gy and mean LMCA dose ≥27 Gy, had significant associations with the risk of major adverse cardiac events.[26] This study also revealed that in patients without congestive heart disease, the LADA volume of dose receiving >15 Gy being ≥10% was an independent estimator of the probability of major adverse cardiac events and all-cause mortality. Higher doses at the base of the heart, near the great vessels (AA,
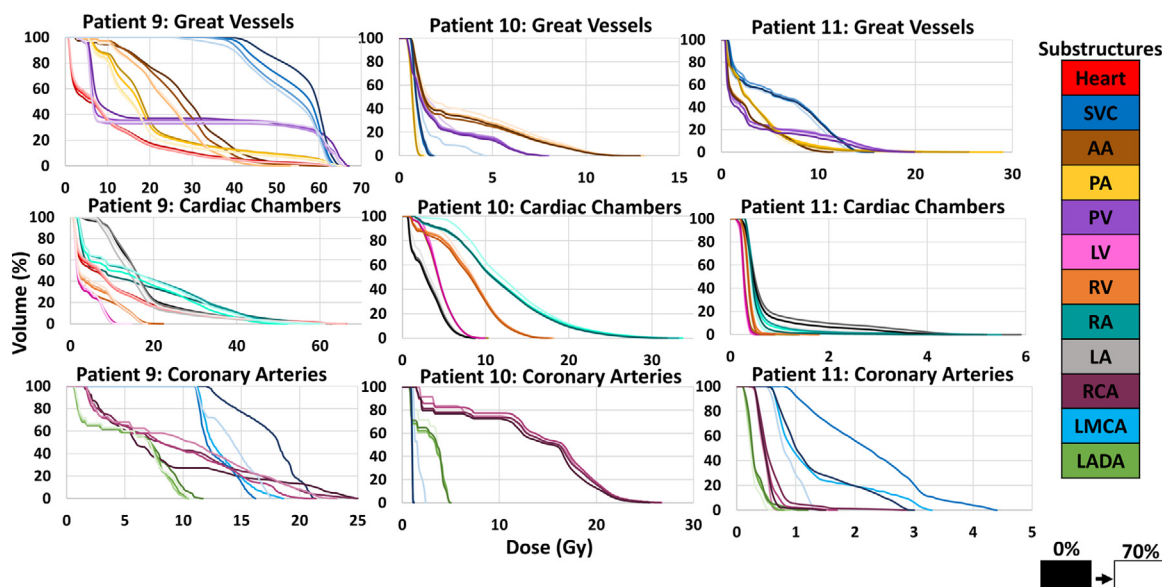

Figure 5 Dose-volume histograms for patients 9, 10, and 11 with lesions in the thoracic region showing the dosimetric variation across respiratory phases for the great vessels (top), the cardiac chambers (middle), and the coronary arteries (bottom). Substructure color gradient transitions from dark to light as the respiratory phases pass from the 0% to the 70% phase, respectively. Cardiac substructure abbreviations are defined in the text. Patient 9 underwent intensity modulated radiation therapy (IMRT) to 60 Gy while patients 10 and 11 received stereotactic body radiation therapy (SBRT) to 50 and 48 Gy, respectively. Note scales adjusted per graph to elucidate changes.

SVC, and PA) have been shown to be associated with worse patient survival,[27] underscoring the importance of establishing accurate substructure safety margins for effective cardiac sparing.

The boxplots shown in Figure 4 for the breast cancer cases highlight that the most dominant differences were observed for the LADA. Notably, doses to the LADA have been linked to increased risk of radiation-induced cardiac morbidity[28] and myocardial infarctions.[29] Recent work by Nicolas et al[30] evaluated cardiac-gated and planning CT scans for 45 patients with left breast cancer and found that LADA movement depended on the location and suggested a safety delineation margin of 10 mm. Other dosimetric endpoints varied based on tumor location, underscoring the importance of patient-specific assessments and robust margin design. Recent work showed the benefits of using cardiac substructure-spared planning in MR-guided RT for improved plan optimization across several thoracic disease sites.[31] Further work in gastro-esophageal junction cancer highlighted the potential benefits of incorporated MRI-guided RT on an MR-linac for cardiac substructure sparing compared with conventional CT-based volumetric modulated arc therapy planning.[32]

One limitation of this work is that only free breathing conditions were evaluated using 4DCT. Deep inspiration breath-hold may be employed to reduce dose to the heart and subsequent cardiotoxicity risk,[33] although evaluation of deep inspiration breath-hold was beyond the scope of this work. The limitation of uncertainties associated with the DIR process (as outlined by American Association of Physicist in Medicine TG 132[34]) was mitigated as segmentations at each phase of respiration were manually verified and corrected. Another limitation is that isolating cardiac excursion was not possible with respiratory-correlated 4DCTs, and thus, the excursions presented in this work represented a contribution from combined respiratory and cardiac motion effects. However, it was reported by Tan et al[35] that the LV and coronary arteries are the most mobile substructures through the cardiac cycle, displacing between 3 to 8 mm between end-diastolic and end-systolic phases. Thus, cardiac motion may be managed through incorporation in future planning organ-at-risk volume design. This work may also be limited in that only 4 phases of the 4DCT were used instead of 10, although characterizing excursion and dosimetric effect for cardiac substructures as well as determining the specific phases where maximum centroid displacement occurred are additional contributions to the literature.

This work included both patients with breast and thoracic cancer, which may have contributed to differing dominant axes of motion from cardiac and respiration influences. Guzhva et al[8] did find that patients with Hodgkin lymphoma had a tendency to have larger displacements in the S-I axis than patients with lung cancer, which could be due to the comorbidities accompanying smoking or otherwise compromised lung function.

Therefore, inconsistencies in patient anatomy could also cause uncertainty in determining the dominant axes of excursion and may be circumvented through expanding the patient cohort or grouping by disease site. This was also observed in patient 3 with abnormal anatomy secondary to scoliosis, which caused the heart and substructures to traverse in predominantly the L-R axes compared with the rest of the cohort where S-I was dominant. Nevertheless, this work was done to validate the need for consideration of cardiac substructures through the incorporation of a motion model. This would provide an opportunity to decrease cardiotoxicity risk during RT.

Conclusion

This work characterized the intrafraction displacement of the cardiac substructures through the respiratory cycle and quantified the potential dosimetric consequences. This work suggests value of cardiac substructure planning organ at risk volume generation to enable more robust cardiac sparing and to reduce the effect of respiration on overall treatment plan quality.

Supplementary materials

Supplementary material associated with this article can be found in the online version at doi:10.1016/j.adro.2021. 100876.

References

1. Hull MC, Morris CG, Pepine CJ, Mendenhall NP. Valvular dysfunction and carotid, subclavian, and coronary artery disease in survivors of Hodgkin lymphoma treated with radiation therapy. *JAMA.* 2003;290:2831–2837.
2. Rutqvist LE, Lax I, Fornander T, Johansson H. Cardiovascular mortality in a randomized trial of adjuvant radiation therapy versus surgery alone in primary breast cancer. *Int J Radiat Oncol Biol Phys.* 1992;22:887–896.
3. Darby SC, Ewertz M, McGale P, et al. Risk of ischemic heart disease in women after radiotherapy for breast cancer. *New Engl J Med.* 2013;368:987–998.
4. van den Bogaard V, Ta B, van der Schaaf A, et al. Validation and modification of a prediction model for acute cardiac events in patients with breast cancer treated with radiotherapy based on three-dimensional dose distributions to cardiac substructures. *J Clin Oncol.* 2017;35:1171.
5. Wong PM, Padley SP. Cardiac computed tomography. *Medicine.* 2018;46:474–479.
6. Wu W, Budovec J, Foley WD. Prospective and retrospective ECG gating for thoracic CT angiography: A comparative study. *Am J Roentgenol.* 2009;193:955–963.
7. Hochhegger B, Marchiori E, Irion K, Souza Jr A, Volkart J, Rubin AS. Magnetic resonance of the lung: A step forward in the study of lung disease. *J Bras Pneumol.* 2012;38:105–115.
8. Guzhva L, Flampouri S, Mendenhall NP, Morris CG, Hoppe BS. Intrafractional displacement of cardiac substructures among

patients with mediastinal lymphoma or lung cancer. *Adv Radiat Oncol*. 2019;4:500−506.

9. George R, Keall P, Kini V, et al. Quantifying the effect of intrafraction motion during breast IMRT planning and dose delivery. *Med Phys*. 2003;30:552−562.

10. Yue NJ, Li X, Beriwal S, Heron DE, Sontag MR, Huq MS. The intrafraction motion induced dosimetric impacts in breast 3D radiation treatment: A 4DCT based study. *Med Phys*. 2007;34:2789−2800.

11. El-Sherif O, Yu E, Xhaferllari I, Gaede S. Assessment of intrafraction breathing motion on left anterior descending artery dose during left-sided breast radiation therapy. *Int J Radiat Oncol Biol Phys*. 2016;95:1075−1082.

12. Morris ED, Ghanem AI, Pantelic MV, Walker EM, Han X, Glide-Hurst CK. Cardiac substructure segmentation and dosimetry using a novel hybrid magnetic resonance and computed tomography cardiac atlas. *Int J Radiat Oncol Biol Phys*. 2019;103:985−993.

13. Morris ED, Ghanem AI, Dong M, Pantelic MV, Walker EM. Glide-Hurst CK. Cardiac substructure segmentation with deep learning for improved cardiac sparing. *Med Phys*. 2020;47:576−586.

14. Feng M, Moran JM, Koelling T, et al. Development and validation of a heart atlas to study cardiac exposure to radiation following treatment for breast cancer. *Int J Radiat Oncol Biol Phys*. 2011;79:10−18.

15. Johnson PB, Padgett KR, Chen KL, Dogan N. Evaluation of the tool "Reg Refine" for user-guided deformable image registration. *J Appl Clin Med Phys*. 2016;17:158−170.

16. Thirion J-P. Image matching as a diffusion process: An analogy with Maxwell's demons. *Med Image Anal*. 1998;2:243−260.

17. Muyan-Ozcelik P, Owens JD, Xia J, Samant SS. Fast deformable registration on the GPU: A CUDA implementation of demons. *International Conference on Computational Sciences and Its Applications, Perugia, Italy, June 30 − July 3,*. IEEE; 2008:223−233.

18. Piper J, Nelson A, Harper J. *Deformable image registration in MIM Maestro evaluation and description*. Cleveland, OH: MiM Software Inc.; 2013.

19. Tong Y, Yin Y, Cheng P, et al. Quantification of variation in dose-volume parameters for the heart, pericardium and left ventricular myocardium during thoracic tumor radiotherapy. *J Radiat Res*. 2018;59:462−468.

20. Fukumitsu N, Nitta K, Terunuma T, et al. Registration error of the liver CT using deformable image registration of MIM Maestro and Velocity AI. *BMC Med Imag*. 2017;17:30.

21. Piper J. SU-FF-I-68: Evaluation of an intensity-based free-form deformable registration algorithm. *Med Phys*. 2007;34:2353−2354.

22. Keall PJ, Mageras GS, Balter JM, et al. The management of respiratory motion in radiation oncology report of AAPM Task Group 76 a. *Med Phys*. 2006;33:3874−3900.

23. Seppenwoolde Y, Shirato H, Kitamura K, et al. Precise and real-time measurement of 3D tumor motion in lung due to breathing and heartbeat, measured during radiotherapy. *Int J Radiat Oncol Biol Phys*. 2002;53:822−834.

24. Wang Y, Bao Y, Zhang L, et al. Assessment of respiration-induced motion and its impact on treatment outcome for lung cancer. *BioMed Res Int*. 2013;2013.

25. Shahid Z, Burns B. *Anatomy, abdomen and pelvis, diaphragm*. StatPearls Publishing; 2019.

26. Atkins KM, Chaunzwa TL, Lamba N, et al. Association of left anterior descending coronary artery radiation dose with major adverse cardiac events and mortality in patients with non-small cell lung cancer. *JAMA Oncol*. 2021;7:206−219.

27. McWilliam A, Kennedy J, Hodgson C, Osorio EV, Faivre-Finn C, van Herk MJEJoC. Radiation dose to heart base linked with poorer survival in lung cancer patients. *Eur J Cancer*. 2017;85: 106−113.

28. Poitevin-Chacón A, Chávez-Nogueda J, Prudencio RR, et al. Dosimetry of the left anterior descending coronary artery in left breast cancer patients treated with postoperative external radiotherapy. *Rep Pract Oncol Radiother*. 2018;23:91−96.

29. Wang X, Pan T, Pinnix C, et al. Cardiac motion during deep-inspiration breath-hold: Implications for breast cancer radiotherapy. *Int J Radiat Oncol Biol Phys*. 2012;82:708−714.

30. Nicolas E, Khalifa N, Laporte C, Bouhroum S, Kirova Y. Safety margins for the delineation of the left anterior descending artery in patients treated for breast cancer. *Int J Radiat Oncol Biol Phys*. 2021;109:267−272.

31. Morris ED, Aldridge K, Ghanem AI, Zhu S, Glide-Hurst CK. Incorporating sensitive cardiac substructure sparing into radiation therapy planning. *J Appl Clin Med Phys*. 2020;21:195−204.

32. Lee SL, Mahler P, Olson S, et al. Reduction of cardiac dose using respiratory-gated MR-linac plans for gastro-esophageal junction cancer. *Med Dosim*. 2020.

33. Welgemoed C, Rogers J, McNaught P, Cleator S, Riddle P, Gujral D. Deep inspirational breath hold to reduce cardiac dose in left-sided breast radiotherapy. *J Radiother Prac*. 2017;16:251−257.

34. Brock KK, Mutic S, McNutt TR, Li H, Kessler ML. Use of image registration and fusion algorithms and techniques in radiotherapy: Report of the AAPM Radiation Therapy Committee Task Group No. 132. *Med Phys*. 2017;44:e43−e76.

35. Tan W, Xu L, Wang X, Qiu D, Han G, Hu D. Estimation of the displacement of cardiac substructures and the motion of the coronary arteries using electrocardiographic gating. *Onco Targets Ther*. 2013;6:1325−1332.